International Journal of Minerals, Metallurgy and Materials
Volume 26, Number 9, September 2019, Page 1129
https://doi.org/10.1007/s12613-019-1820-y

Solid solution evolution during mechanical alloying in Cu–Nb–Al compounds

Kaouther Zaara[1)], *Mahmoud Chemingui*[1)], *Virgil Optasanu*[2)], *and Mohamed Khitouni*[1)]

1) Laboratory of Inorganic Chemistry, UR 11-ES-73, University of Sfax, B.P. 1171, Sfax 3018, Tunisia

2) ICB, UMR 6303 CNRS, University of Bourgogne Franche Comté, 9 av. Alain Savary, 21078 Dijon Cedex, France

(Received: 31 October 2018; revised: 8 December 2018; accepted: 13 December 2018)

Abstract: This work concerns the structural evolution of $Cu_{70}Nb_{20}Al_{10}$ (at%) alloy processed by mechanical alloying using a planetary ball mill in air atmosphere for different times (4 to 200 h). The morphological, structural, microstructural, and thermal behaviors of the alloy were investigated by scanning electron microscopy, energy-dispersive spectroscopy, X-ray diffraction, and differential scanning calorimetry. X-ray diffraction patterns were examined using the Rietveld refinement technique with the help of the MAUD software. A disordered FCC-Cu(Nb,Al) solid solution was formed after 8 h of milling. The crystallite size, microstrain, and lattice parameter were determined by the Rietveld method. With increasing milling time, the crystallite size of the final product—ternary-phase FCC-Cu(Nb,Al)—is refined to the nanometer scale, reaching 12 nm after 200 h. This crystallographic structure combines good mechanical strength and good ductility. An increase in microstrain and partial oxidation were also observed with increasing milling time.

Keywords: powder metallurgy; mechanical alloying; nanomaterials; copper-based alloy; solid solution

1. Introduction

Introduced in the early 1970s [1], mechanical alloying (MA) is a very popular technique for producing alloy powders. This process is widely applied to the production of compounds with a high energy of mixing, supersaturated solid solutions, and alloys of elements whose equilibrium phase diagrams do not indicate a noticeable solubility [1–4]. The production of alloys from immiscible metal systems can be achieved also by rapid solidification (RS), where two phases can be produced in a fine distribution; however, RS cannot produce solid solutions with high metal content. In fact, RS can produce alloys in a thin ribbon shape, which are frequently fragile and difficult to consolidate. By contrast, solid solutions with high metal content and alloys with good homogeneity are easily prepared via the MA process. Also, MA enables the production of alloys in powder form that can consolidate or be compacted easily, making them attractive for many practical applications. The repeated fracturing and cold welding of the particles that occur during the MA process lead to reactions between the components of the elemental powder mixture as well as to a high density of dislocations and a large number of grain boundaries [5–6].

The mechanical and physical properties of nanocrystalline materials are known to directly depend on their microstructural parameters. These parameters can be analyzed by X-ray diffraction (XRD) using various techniques [7–10]. The Rietveld method is a full-pattern fitting technique that is very useful for microstructural characterization. This method gives the best results for microstructure characterizations and quantitative estimations of multiphase materials whose diffraction patterns include multiple overlapping reflections [11–12].

Cu-based nanocrystalline and amorphous materials have shown excellent mechanical properties and high electrical and thermal conductivities; they are therefore appropriate for use in the welding industry and in electrical applications [13]. Because of these advantages, numerous investigators have studied the relation between mechanical properties and microstructure of Cu-based nanocrystalline and amorphous materials [14–16]. The Cu–Nb system is an example of a binary immiscible metal system [17]. This alloy was first obtained by MA by Morris and Morris [18] and then by Benghalem and Morris [19]. Botcharova *et al.* [20–21]

Corresponding author: Virgil Optasanu E-mail: virgil.optasanu@u-bourgogne.fr

have demonstrated that Nb can be dissolved homogeneously within the Cu matrix at concentrations as high as 10at% by MA. The formation of a complete solid solution for the Cu–20%Nb composition was not achieved, likely because of the very high Nb content and the short milling time (17 h). Recently, Mula *et al.* [22] and Lei *et al.* [23] have discussed the formation of Cu–Nb solid solutions, noting that the kinetics of the alloying process in Cu–Nb systems is not yet understood.

In the literature, the influence of the milling environment on the powder obtained at the end of the MA process has not been widely studied. Azabou *et al.* [24] and Khitouni *et al.* [25] reported that a stable copper oxide phase could be obtained by MA under an air atmosphere. Yoon *et al.* [26] have studied the influence of different milling atmospheres on the thermoelectric and mechanical properties of Bi–Sb–Te alloys. They found good thermoelectric properties in the alloy prepared by MA under an Ar atmosphere and a high hardness value after the powder milled under an air atmosphere was sintered. Zhao *et al.* [27] have synthesized a Cu–3.6vol%Al_2O_3 dispersion-strengthened alloy by MA of internal oxidation Cu–Al powders. They used internal oxidation of Cu–Al powders (by mixing and subsequently heating Cu–Al with Cu_2O powders) followed by milling under an air or Ar atmosphere to obtain nanometric Al_2O_3 oxides dispersed in a Cu matrix to enhance the mechanical properties and maintain the good electrical characteristics. They optimized the time of milling compared with classic MA techniques. The finally compacted alloy exhibited excellent mechanical and electrical properties because of the complete oxidation of residual Al as reinforcing particles.

The aim of the present work is to synthesize $Cu_{70}Nb_{20}Al_{10}$ by MA. Very few researchers have studied this system. Silva and Lima [28] synthesized the Cu–13Al–2Nb (wt%) shape-memory alloy under an Ar atmosphere and at a rotation rate of 150 r/min for 65 h for further memory-shaping purposes. In the present study, we work with a sensibly higher content of Nb and use different processing parameters such as very long milling times and an air atmosphere. We detailed here the effect of the milling time on the evolution of microstructural parameters, including the crystallite size, microstrain, and the lattice parameter, by using Rietveld refinement of XRD patterns. In addition, we studied the thermal behavior exhibited at the end of the milling. The techniques used for these purposes were scanning electron microscopy (SEM), XRD, and differential scanning calorimetry (DSC).

The Cu–Nb–Al system was chosen because Cu-based nanocrystalline materials exhibit excellent thermal, electrical, and mechanical proprieties. In addition, Al is a good candidate to achieve a supersaturated Cu–Nb–Al solid solution by MA because of its smaller atomic radius compared with those of Cu and Nb, which enables it to dissolve into the Cu matrix at an early stage of milling. By decreasing the matrix grain size to the nanometer scale, the mechanical properties can be improved. In addition, good hardening properties can be achieved through homogeneous distribution of the alloying elements in the solid solution.

2. Experimental

Ternary Cu–Nb–Al powder alloys with nominal atomic composition $Cu_{70}Nb_{20}Al_{10}$ were prepared in a planetary ball mill (Fritsch Pulverisette P7). The initial elemental powders had different size distributions in the range 40–74 μm. The elemental powders of Cu (99.99%), Nb (99.85%), and Al (99.9%) were precisely weighed to give the desired nominal compositions. The synthesis was carried out using a hardened chromium steel vial with five chromium steel balls (diameter 10 mm) under an air atmosphere. The MA was carried out at 600 r/min and with a ball-to-powder mass ratio of 2:1. The total period of the process was 200 h. The process was performed in a periodical sequence of 10 min of milling followed by 5 min of pause to refresh the vials and avoid local heating. A small amount of powder was collected for characterization after different milling times.

Structural investigations of the milled powders were carried out on an X'Pert High Score Plus diffractometer in θ–2θ geometry using Cu K_α radiation generated at 40 kV and 40 mA. The existing phases were identified using the High Score Plus program based on the ICDD PDF2 database. The average microstructure parameters were evaluated through refinement of the XRD patterns with the help of the MAUD software [29]. The morphology of the powder particles was observed with a scanning electron microscope (Hitachi SU1510, Japan). The chemical composition was studied by energy-dispersive spectroscopy (EDS). Finally, thermal analysis was carried out by DSC (Netzch STA 449 C Jupiter, Germany) from 20 to 700°C (at 10°C/min heating and cooling rates) under an Ar atmosphere.

3. Results and discussion

3.1. Morphological evolution

Fig. 1 reveals the evolution of the morphology of the $Cu_{70}Nb_{20}Al_{10}$ powder mixture milled for different times. The particles of the elemental powder mixture were approximately

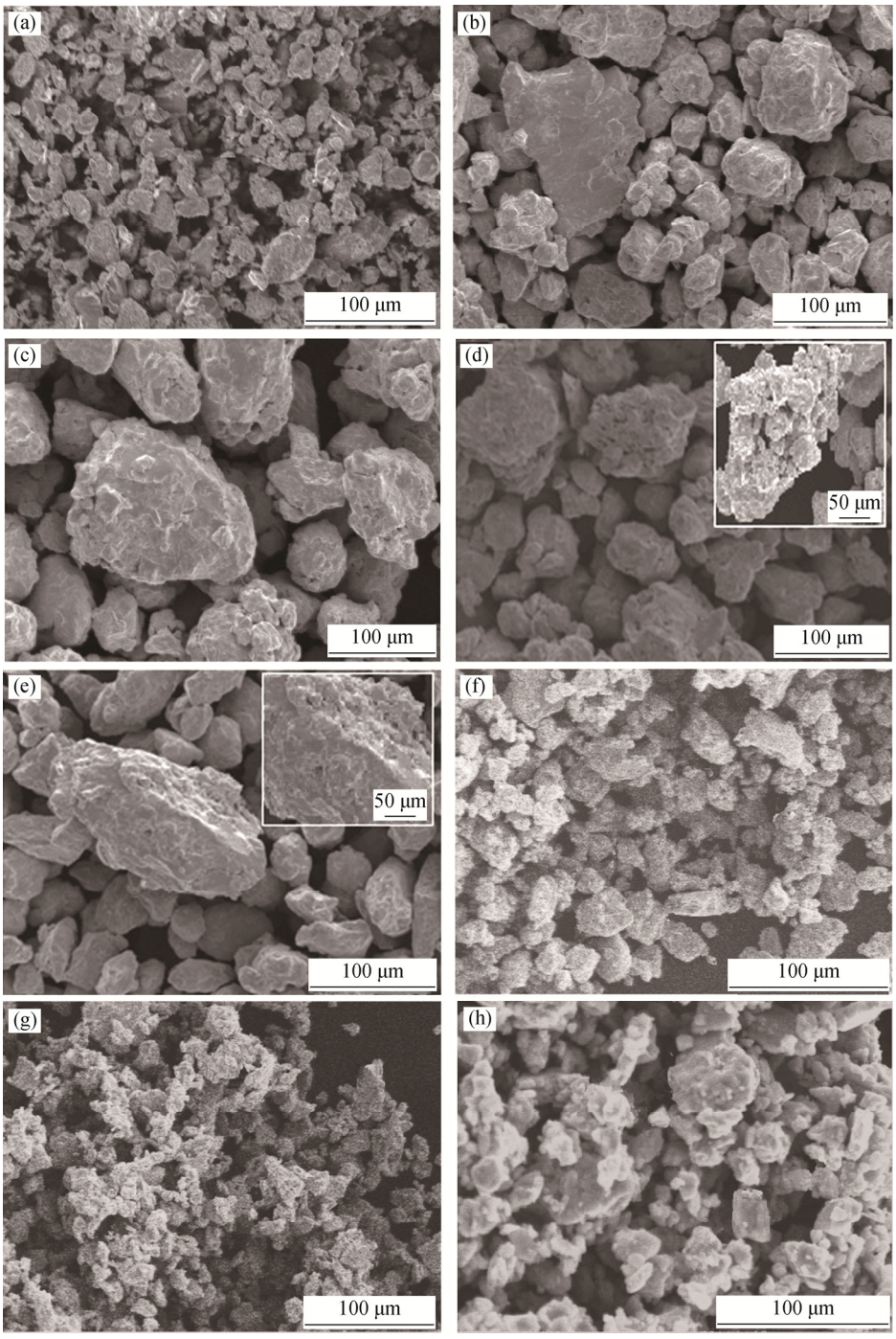

Fig. 1. SEM images of the $Cu_{70}Nb_{20}Al_{10}$ powder mixture mechanically milled for different times: (a) 0 h; (b) 16 h; (c) 20 h; (d) 30 h; (e) 50 h; (f) 80 h; (g) 110 h; (h) 200 h.

spherical, with an average size in the range 40–70 μm (Fig. 1(a)). An increase in particle size was observed after 16 h of milling, with an average of 10–156 μm. This increase in particle size was due to the predominance of the welding phenomenon against fracturing. The flat shape observed for some powder particles (Fig. 1(b)), where some of the particles were substantially larger than the initial size, suggests the occurrence of cold welding due to the strong compressive forces during the ball–powder–ball collisions. Strong plastic deformation must have occurred to produce substantial morphological modification of the grains. After 20 h of milling, the particle size continued to increase, reaching an average of 43–180 μm (Fig. 1(c)). After 30 h of milling, the average particle size reached 39–175 μm and agglo-

merated particles were observed (Fig. 1(d)). Agglomerated particles obtained by cold welding of smaller particles were also observed after 50 h of milling (Fig. 1(e)). The estimated agglomerate size is approximately 190 μm, indicating that the welding effect was predominant. The presence of small particles indicates that the fracturing process also occurred. After 80 h of milling, the particles became finer and more homogeneous as a result of the predominance of the fracture process. A rapid decrease in particle size to 15–45 μm was observed at this stage (Fig. 1(f)). This rapid decrease might be due to the accumulation of defects and the strong hardening of the material during the milling process. A steady state was observed when the milling time was increased to 110 and 200 h, with an average particle size in the range 2–23 μm (Figs. 1(g) and 1(h), respectively).

The EDS analysis corresponding to 80 h of milling is given in Fig. 2(a). The images confirm the homogeneous distribution of Cu, Nb, and Al in the mechanically alloyed powder. The results of the chemical composition analysis of the individual particles were found to be in good agreement with the nominal composition of the powder mixture (68.84at%Cu–21.47at%Nb–8.16at%Al). Also, the EDS analysis indicates traces of Fe (1.21at%) and Cr (0.295at%), which possibly originate from the chromium steel balls used in the ball-milling process. Figs. 2(b) and 2(c) present the EDS mapping images for Cu, Nb, and Al and show a homogeneous distribution of Nb and Al in the Cu matrix.

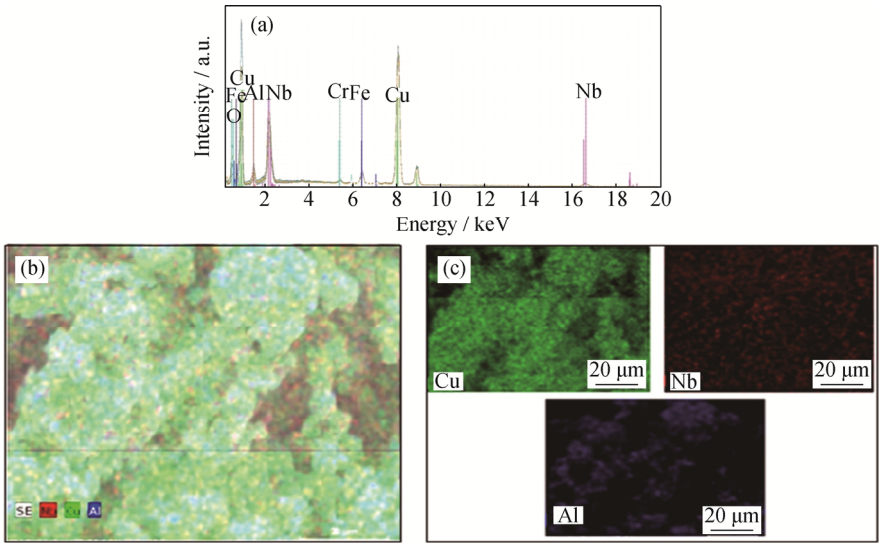

Fig. 2. (a) EDS spectrum of $Cu_{70}Nb_{20}Al_{10}$ and (b, c) EDS mapping images of the base elements in $Cu_{70}Nb_{20}Al_{10}$ powder milled for 80 h.

3.2. X-ray diffraction analysis

The formation of nanocrystalline and/or amorphous alloy powders by MA is strongly dependent on the processing parameters. The most important processing parameters are the milling time, milling atmosphere, ball-to-powder ratio, and rotation speed. In our study, we changed only the milling time while keeping the other parameters constant. The XRD patterns of the investigated $Cu_{70}Nb_{20}Al_{10}$ powder after different milling times are presented in Fig. 3, where the diffractogram of the unmilled powder mixture is also included for comparison. The broadening of the diffraction peaks and the decrease of their intensities indicate the introduction of various structural defects such as grain boundaries, vacancies, and stacking faults, as well as a decrease of the crystallite size. The existence of various crystal defects facilitates the diffusion of elementary compounds. As a result, the structural changes can occur through solid-solution diffusion (resulting in the disappearance of certain peaks) and/or the formation of new phases (the appearance of new peaks) [5].

The XRD pattern of the initial powder mixture (0 h) indicates a face-centered cubic (FCC) structure for Cu and Al and a body-centered cubic (BCC) structure for Nb, with corresponding lattice parameters of a_0 = 0.3611(1) nm, a_0 = 0.4051(2) nm, and a_0 = 0.3303(1) nm, respectively. Even after a short milling time (4 h), the XRD peaks broadened and their intensity sharply decreased as a result of the internal strain increase and crystallite size reduction. Heavy deformations and the repeated fracturing of the powder particles are responsible for the microstructural changes during

MA [30–31]. However, as shown in Fig. 3, all of the peaks of crystalline Al disappeared completely. This complete disappearance corresponds to the complete dissolution of Al atoms into the FCC-Cu matrix. The melting point of the solute is widely known to provide information about the diffusivity: the lower the melting point, the higher the diffusivity [32]. On the one hand, according to the thermodynamic data, Nb has a higher melting temperature (2477 °C) than Al (660.32 °C) [31]. On the other hand, the Cu peak is displaced slightly toward smaller angles left (from 43.39° to 43.32°). This displacement indicates that an increase in the cell parameter of Cu occurred because of the dissolution of Al. The lack of superlattice diffraction peaks shows that the crystalline Cu(Al) phase has a disordered structure. As a result, a disordered Cu(Al) solid solution was formed by mixing elemental powders Cu and Al, which possess the same structure type as the FCC-Cu. Similar observations have been reported for Fe–Al [33–34], Fe–Co [35], Cu–Al [36], and Ni–Al [37]. Compared with the similar composition Cu–Al–Nb milled under an Ar atmosphere [28], the Cu(Al) phase in our work, which was prepared under an air atmosphere, was obtained earlier (after 4 h). After 8 h of milling, a strong decrease in the Nb peak intensities and a strong shift of the Cu peak at 43.32° to a smaller angle (43.07°) were observed, along with a lack of superlattice diffraction peaks. These observations demonstrate that Nb gradually reacted with FCC-Cu(Al) to form a disordered Cu(Nb,Al) solid solution with the same structure type as the FCC-Cu. After 12 h of milling, the peaks of Cu(Nb,Al) and Nb exhibited broadening and a decrease in intensity. The XRD patterns of the powders mechanically alloyed for 16, 20, and 30 h do not differ from the pattern obtained after 12 h of milling. Only the Nb peaks continue to broaden and decrease in intensity with increasing milling time. After 50 h, only a very weak (110)-Nb peak exists, which illustrates that, at this point, a small amount of Nb atoms have still not dissolved into the Cu matrix (Fig. 3).

After 80 h of milling, all of the Nb peaks disappear and only the peaks related to the FCC-Cu(Nb,Al) solid solution and some other peaks are visible. These peaks correspond to the identified monoclinic fine phase of CuO. The XRD patterns of the samples subjected to prolonged milling (110 and 150 h) also show the existence of a CuO phase. After 200 h, the XRD patterns present the same phases, with an increase in intensity of the CuO peaks (Fig. 3). The formation of copper oxide at these stages is due to the absorption of oxygen at the powder surface during milling [38]. The atmosphere environment and the high reactivity of the surfaces of particles are other causes of the continuous oxidation with increasing milling time.

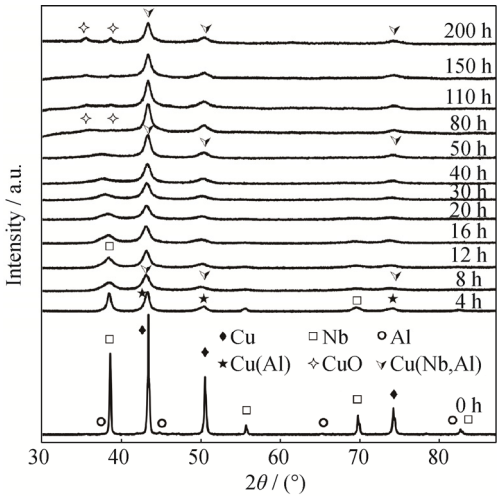

Fig. 3. XRD patterns of $Cu_{70}Nb_{20}Al_{10}$ powder as a function of mechanical alloying time.

Another feature in Fig. 3 is the change in position of the main (111)-Cu diffraction peak with increasing milling time. At milling times between 4 and 20 h, the peak shifted to lower 2θ values. This shift is explained by the formation of solid solutions and the expansion of the lattice parameter of Cu. With additional milling time, the angular shift of the Cu main diffraction peak, (111), toward higher values (reaching $2\theta = 43.29°$ after 40 h) may be due to the substitution of Nb atoms in the Cu matrix and the consequent decrease of the lattice parameter of Cu. At milling times between 50 and 200 h, the positions of the 2θ peaks of Cu remain relatively unchanged.

Fig. 4(a) shows the Rietveld refinement results for the XRD pattern of the powder mixture before milling, which was prepared by combining three raw materials: FCC-Cu, BCC-Nb, and FCC- Al. After 4 h of milling, the Rietveld refinement was obtained by introducing three phases: FCC-Cu, BCC-Nb, and FCC-Cu(Al) solid solution (Fig. 4(b)). After 8 h (Fig. 4(c)), the XRD pattern shows a strong decrease in intensity of the Nb diffraction peaks, leading to the formation of the FCC-Cu(Nb,Al) solid solution. The continuous dissolution of Nb into the Cu matrix was observed after 12 h of milling (Fig. 4(d)). After 50 h of milling (Fig. 4(e)), the Rietveld refinement was performed with two phases introduced: the FCC-Cu(Nb,Al) solid solution and the Nb phase. After 80 h (Fig. 4(f)), the CuO phase (space group: $C2/c$; $a = 0.468$ nm; $b = 0.342$ nm; $c = 0.513$ nm [25]) was revealed by Rietveld refinement; this phase remained after 200 h of milling (Fig. 5).

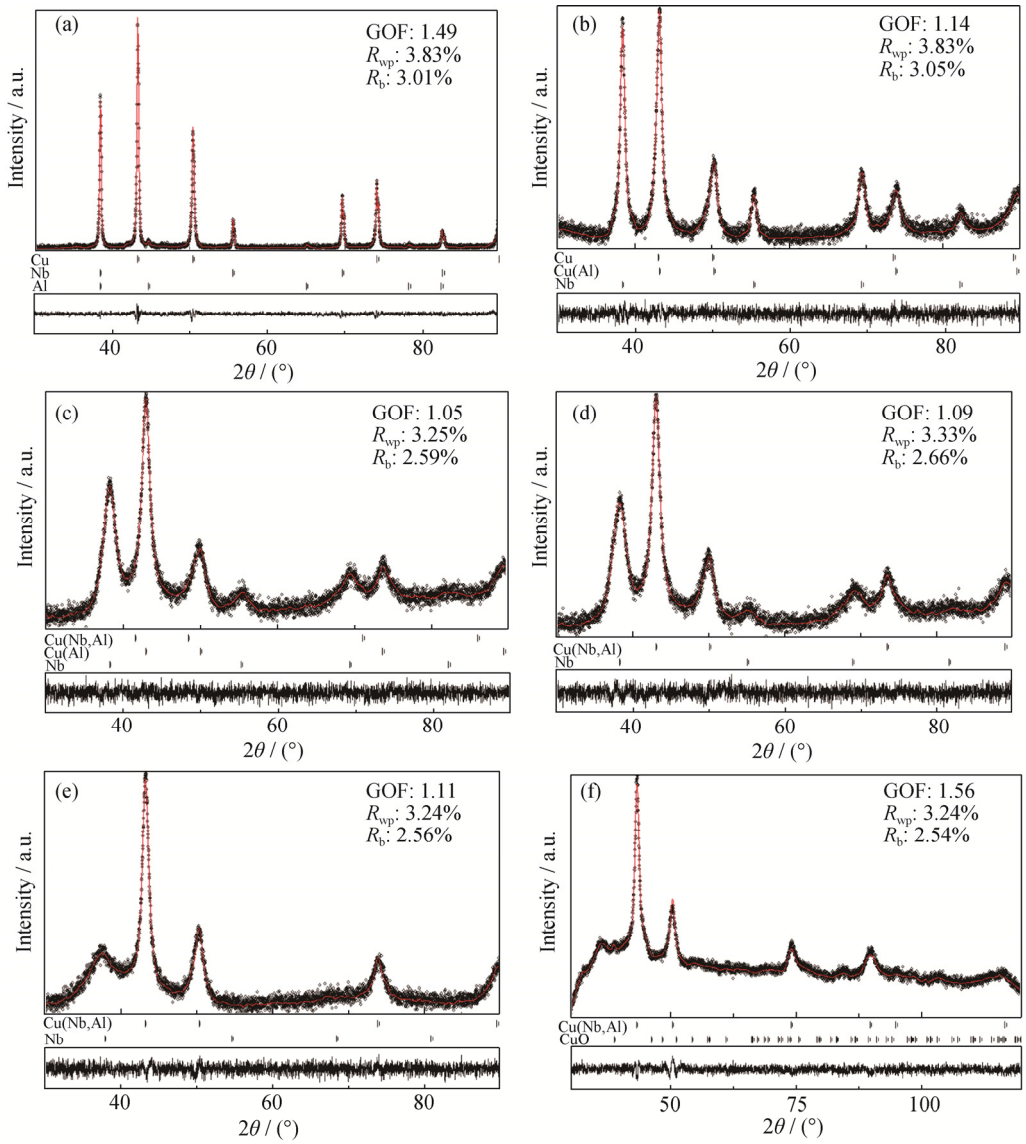

Fig. 4. Rietveld refinement of the XRD pattern of the $Cu_{70}Nb_{20}Al_{10}$ powders milled for different times: (a) 0 h; (b) 4 h; (c) 8 h; (d) 16 h; (e) 50 h; (f) 80 h. Experimental (dots) and calculated (full line) patterns are shown. GOF—Goodness of fit; R_{wp}—Weighted profile *R*-factor; R_b—Bragg intensity *R*-value.

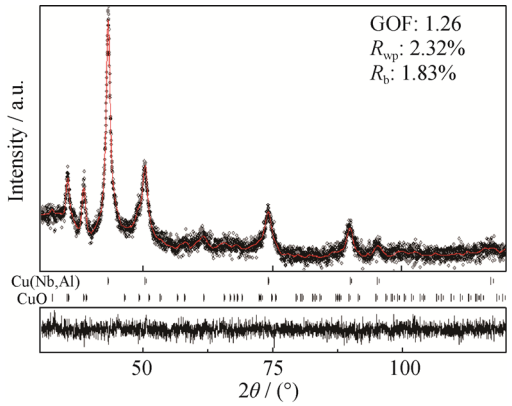

Fig. 5. Rietveld refinement of the XRD pattern of the powders milled for 200 h. Experimental (dots) and calculated (full line) patterns are shown.

Fig. 6 shows the evolution of the phase proportions during the milling. A decrease of the Cu phase proportion is observed at an early stage of processing. An increase in the fraction of the Cu(Al) to approximately 17wt% and a decrease of the fraction of the Nb to approximately 31wt% are visible after 8 h. The phase proportion of Cu(Nb,Al) increases with increasing milling time, reaching a value of 96wt% after 50 h of milling; by contrast, the Nb proportion continuously decreases, reaching a very low value after 50 h of milling. With additional milling time, the phase proportion of FCC-Cu(Nb,Al) decreases slightly but continuously because of its partial oxidation, reaching values of 86wt% after 80 h and 74wt% after 200 h of milling. The CuO phase proportion is 14% after 80 h of milling, then increases con-

tinuously to 26wt% after 200 h.

In our study, CuO was observed after prolonged milling time, in contrast to other studies, where it was detected at an early stage of milling [24–25]. This discrepancy can be attributed to the Al and Nb affecting the Cu matrix before the incorporation of oxygen.

Suryanarayana [5] demonstrated that metastable phases produced by MA can present attractive combinations of chemical, electrical, mechanical, and magnetic properties and can be used in numerous applications.

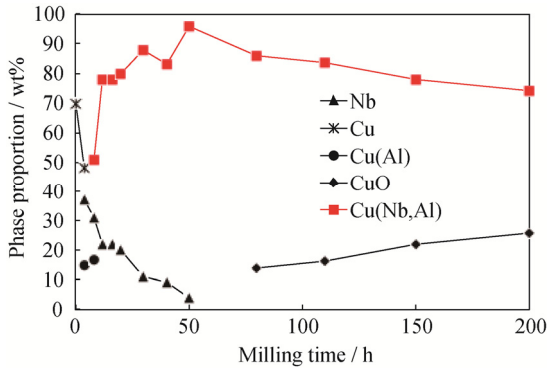

Fig. 6. Phase proportion evolution as a function of the milling time.

3.3. Evolution of lattice parameters and microstrain

Fig. 7 shows the evolution of the lattice parameters of the Cu, FCC-Cu(Al), Nb, and FCC-Cu(Nb,Al) solid solution during the milling process. During the first 4 h of milling, the Cu lattice parameter increases slightly from its initial value of approximately 0.363 nm. The lattice parameter of the newly created FCC-Cu(Al) after 4 h is smaller than that of Cu, reaching 0.3621(1) nm. After 8 h, the lattice parameter of FCC-Cu(Al) increases to approximately 0.3641(1) nm. This increase is correlated with the shift of the peak to smaller 2θ angles (see Fig. 3) and is related to the dissolution of a large amount of Al atoms into the Cu matrix. A rather large lattice parameter of $a = 0.3661(2)$ nm was observed for the new solid solution FCC-Cu(Nb,Al) after 30 h of milling; this large value is attributable to the dissolution of Nb, which has a larger atomic radius than Cu. A strong decrease of this lattice parameter is observed after 50 h, reaching a minimum of $a = 0.3615(1)$ nm. Similar observations of a decrease of the lattice parameter between 30 and 50 h of milling were reported by both Botcharova *et al.* [20] and Abad *et al.* [39]. This decrease is explained by the induced structural defects and/or by the insertion of oxygen atoms at the interstitial sites of the Cu lattice. Another possible explanation is the formation of niobium and aluminum oxide nanoparticles not detectable by XRD [20–21] and resulting from the precipitation of Nb and Al from the supersaturated solution. The lattice expansion/contraction can also be assigned to vacancies or to point defects in the crystallites.

Fig. 7 also shows a continuous increase of the Nb lattice parameter over the first 30 h of milling, a period where it remains constant, and then the disappearance of the Nb phase. This initial expansion may be due to increases in the density of lattice defects (dislocations) with their characteristic strain fields at the nanograin boundary or to interdiffusion between Cu and Nb. Abad *et al.* [39] and Pfeiler [40] have noted that large amounts of Cu (up to 25at%) can be dissolved in Nb, which is likely one of the reasons behind the increase in the Nb lattice parameter observed in the present work.

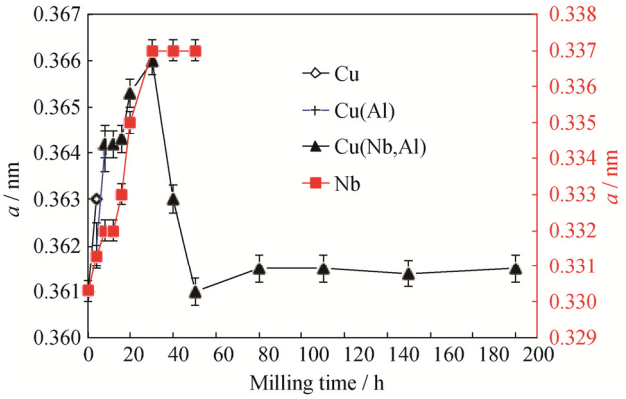

Fig. 7. Lattice parameter evolution as a function of the milling time. The Nb lattice-parameter values are reported on the secondary vertical axis.

The refinement of the XRD patterns with the MAUD program gives an estimation of the crystallites' size and microstrain. Fig. 8 shows the variations of crystallite size and microstrain for the powder alloy Cu(Nb,Al) as a function of the milling time. The crystallite size of FCC-Cu(Nb,Al) powder decreases sharply from its initial value of 82 nm after 8 h to 20 nm after 12 h of milling. The average crystallite size reaches a minimum of nearly 12 nm after 30 h of milling. With further milling, the refining of the powder tends to become well-balanced, resulting in the crystallite size remaining constant at approximately 12 nm for longer milling times (up to 200 h). This reduction of the crystallite size is due to the new defects formed, such as dislocations and pileup of grain boundaries in untidy clusters within the crystallites. In general, some properties can be improved when the crystallite size is reduced to the nanoscale by severe plastic deformation. Lei *et al.* [41] have demonstrated that

the mechanical and electrical properties of Cu–Nb alloys after the hot-pressing process are strongly dependent on their microstructure. First, the high strength is related to the nanocrystalline grains responsible for grain-boundary strengthening. Second, the electrical conductivity is influenced by the grain size of the Cu. We therefore expected our material to exhibit very good mechanical and electrical properties after consolidation.

The microstrain, by contrast, shows a gradual increase over the first 80 h of milling up to 0.50%, followed by a slight increase, reaching a value of 0.58% at the end of milling. These results indicate that the MA process with the repeated fracturing and cold welding not only refines the powder but also causes substantial microstrain and therefore increases dislocations in the powder crystals and leads to a high rate of grain-boundary formation.

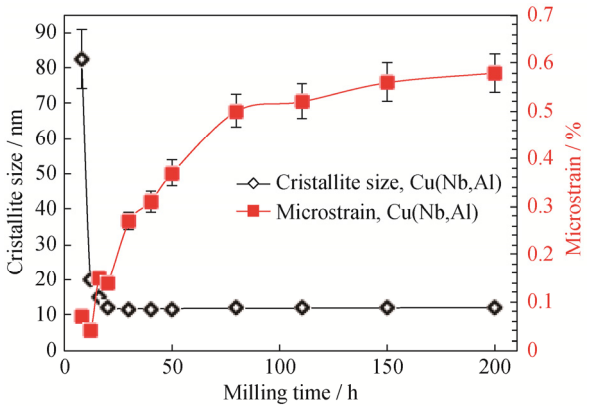

Fig. 8. Evolution of the microstructure parameters of the FCC-Cu(Nb,Al).

Fig. 9 shows the variation of the crystallite size of the Cu, Nb, and Cu(Al), as well as the microstrain of the Nb and Cu(Al). For the Cu, the crystallite size decreases slightly to <75 nm after 4 h. Slimi *et al.* [42] have reported similar observations. The Nb and the FCC-Cu(Al) crystallite size rapidly decrease after 8 h of milling to approximately 9.4 nm and 10.6 nm, respectively. With further milling, the crystallite size of Nb decreases progressively to approximately 8.0 nm after 40 h and 7.7 nm after 50 h of milling. After 8 h of milling, the microstrain of FCC-Cu(Al) reaches 0.07%. In the case of Nb, the microstrain increases gradually until 16 h of milling and reaches 0.36% after 50 h of milling. The increase of the microstrains during MA is a result of the stress fields associated with the multiplication of dislocations and with the introduction of impurities, vacations, antisite defects, dislocations, and other lattice defects during milling [43].

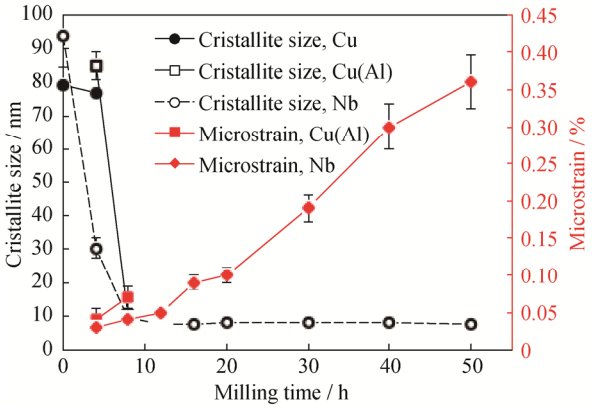

Fig. 9. Evolution of the microstructure parameters of Cu, Nb, and Cu(Al).

In the MA process, the powders are subjected to severe plastic deformation; thus, a large number of crystallite defects are introduced. The dislocations are the main defects besides grain boundaries. The dislocation density (ρ_D) of $Cu_{70}Nb_{20}Al_{10}$ can be estimated on the basis of the Rietveld method. The dislocation density can be represented by the following equation [44]:

$$\rho_D = 2\sqrt{3}\frac{(\varepsilon^2)^{\frac{1}{2}}}{Db} \quad (1)$$

where ε is the microstrain, D is the crystallite size, and b is the Burgers vector. In the case of FCC materials, cold plastic deformation is caused by the emergence and slip of dislocations on {111} close-packed planes and in <110> close-packed directions [45]. Thus, the Burgers vector of $Cu_{70}Nb_{20}Al_{10}$ in direction [110] is equal to $\frac{a}{2}\sqrt{2}$, where a is the lattice parameter corresponding to the duration of each milling. According to Slimi *et al.* [46], the maximum ρ_D of milled Cu–Fe–Ni is approximately 6×10^{15} m^{-2} after 100 h of milling. Fig. 10 gives the variation of the dislocation density ρ_D of $Cu_{70}Nb_{20}Al_{10}$ powders, as calculated using Rietveld refinement, as a function of the MA duration. The ρ_D values rapidly increased from approximately 0.063×10^{16} m^{-2} to approximately 3.23×10^{16} m^{-2} during the first 30 h of milling. As expected, the dislocation density increases rapidly in the early stage of milling because of the severe plastic deformation. With further milling (>30 h), the ρ_D gradually increases to 5.69×10^{16} m^{-2} after 80 h of milling and then remains relatively unchanged. A steady-state value of approximately 6.43×10^{16} m^{-2} was observed after 200 h of milling. The milling time appears to be the major experimental parameter: the longer the milling time, the higher the dislocation density value.

The hardness of the alloys is strongly increased by the

formation of a nanocrystalline, supersaturated solid solution, and also by the presence of a high density of defects and high residual stress in the grains of the powder. Thus, from the aforementioned observations, high microhardness values are expected.

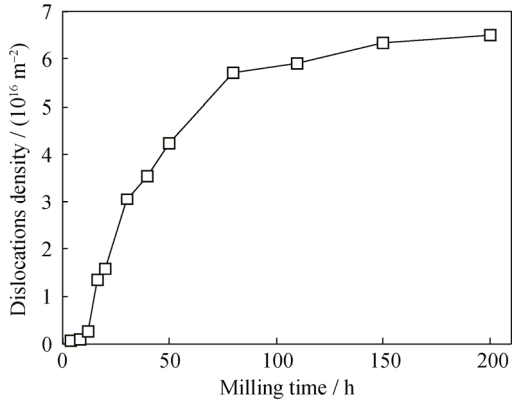

Fig. 10. Evolution of the dislocation density as a function of the milling time.

3.4. Preliminary DSC study

To evaluate the stability of the milled powder for further hot compaction purposes, the thermal behavior of the $Cu_{70}Nb_{20}Al_{10}$ powder milled for 200 h was investigated by DSC. We used continuous heating and cooling at a rate of 10°C/min under an Ar atmosphere. The DSC curve corresponding to 200 h of milling is shown in Fig. 11. The DSC curve is characterized by a series of three exothermic events. The first broad exothermic event was observed between 200 and 360°C with a maximum at 293.7°C and an enthalpy of 38.85 J/g. This event can be attributed to the partial decomposition of the CuO within the presence of Al and Nb and to further form alumina (Al_2O_3) or niobium oxide (Nb_2O_5) because of their low enthalpy of formation [47–48]. Conceivably, this peak could represent a combination of several phenomena. Indeed, at this temperature, the recovery of defects introduced by the MA is thermally activated. The second exothermic event occurs between 390 and 520°C with a maximum at 483.7°C and an enthalpy of 13.01 J/g. This event is most likely related to the decomposition of the FCC-Cu(Nb,Al) supersaturated solid solution to AlCu, Al_2Cu, or Al_4Cu_9. To the best of our knowledge, AlCu is the most thermally stable of these phases. Moreover, because our matrix is Cu, the formation of Al_2Cu or Al_4Cu_9 is unlikely. The third broad exothermic peak was observed in the range between 520 and 620°C with a maximum at 579.3°C and an enthalpy of approximately 5.03 J/g. This event is possibly characteristic of the formation of an intermediate compound Al_3Nb, which is a very stable phase [49]. The cooling stage of the DSC curve shows that the powder did not suffer any reversible reaction.

Further systematic studies concerning the reactions and transformations during the heating as well the consolidation of the powder by SPS are in progress and will be published separately.

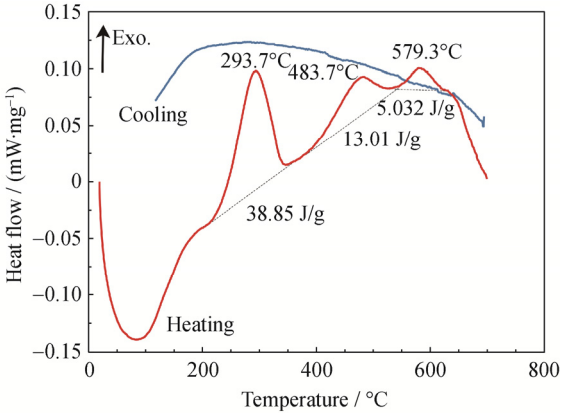

Fig. 11. Typical DSC scans for $Cu_{70}Nb_{20}Al_{10}$ alloy after 200 h of milling at a heating rate of 10°C/min.

4. Conclusions

The $Cu_{70}Nb_{20}Al_{10}$ compound was synthesized by MA. The effect of milling time on the morphology, structural changes, microstructural characteristics, and thermal behavior of mechanically alloyed $Cu_{70}Nb_{20}Al_{10}$ powders was investigated, and the following results were obtained.

(1) The high-energy milling of $Cu_{70}Nb_{20}Al_{10}$ powder mixtures leads to the formation of a FCC-Cu-based solid solution. This crystallographic structure ensures high mechanical strength and good ductility.

(2) The nanocrystalline Cu(Nb,Al) solid-solution powder shows a crystallite size of approximately 12 nm after 200 h of MA.

(3) The morphology and size distribution of the powder particles change during MA. In the early stage of milling, the average particle size of the powder elements increases progressively. This increase is also accompanied by the accumulation of internal strains. The Cu–Nb–Al nanocrystalline powder particles become uniform in size and round shaped with further milling.

(4) At the early stage of the MA process, both the Cu(Al) solid solution formed after 4 h and the resulting powder show a nanometric-scale structure. When the milling time is 8 h, the ternary FCC-Cu(Nb,Al) starts to form. At longer milling times, all of the Nb atoms dissolve into the Cu(Al) lattice and the formation of the Cu(Nb,Al) is completed. A cupric oxide was revealed by XRD after 80 h of milling.

The XRD patterns of these phases were successfully analyzed with the help of the MAUD program by employing the Rietveld refinement technique. The dislocation densities were found to be 6.43×10^{16} m^{-2}, and the strain broadening caused by high-energy MA is consistent with the concept of dislocations.

(5) DSC curves of the nanocrystalline Cu–Nb–Al powder show three exothermic peaks. These exothermic peaks were speculated to be caused by the formation of Al_2O_3 and (likely) Nb_2O_5 oxides, the AlCu stable phase, and the Al_3Nb phase.

(6) This investigation has shown that MA is a promising way of producing nanocrystalline materials with very good properties, such as high strength and hardness superior to that of conventional materials.

The compound was studied here from the viewpoint of its microstructure. Future research will be devoted to consolidating the powders and then studying their mechanical, thermal, and electrical properties. After optimization, this family of compounds may be useful for industrial applications such as welding or as electrical conductors with high mechanical strength (after heat treatments), as required for pulsed high-field magnets. Consolidation experiments using the spark plasma sintering method are underway.

References

[1] J.S. Benjamin, Dispersion strengthened superalloys by mechanical alloying, *Metall. Trans.*, 1(1970), No. 10, p. 2943.

[2] A.R. Yavari, P.J. Desré, and T. Banameur, Mechanically driven alloying of immiscible elements, *Phys. Rev. Lett.*, 68(1992), No. 14, p. 2235.

[3] K. Uenishi, K.F. Kobayashi, S. Nasu, H. Hatano, K.N. Ishihara, and P.H. Shingu, Mechanical alloying in the Fe–Cu system, *Z. Metallkd.*, 83(1992), No. 2, p. 132.

[4] J. Kuyama, H. Inui, S. Imaoka, K.N. Ishihara, and P.H. Shinhu, Nanometer-sized crystals formed by the mechanical alloying in the Ag–Fe system, *Jpn. J. Appl. Phys.*, 30(1991), No. 5A, p. L854.

[5] C. Suryanarayana, Mechanical alloying and milling, *Prog. Mater. Sci.*, 46(2001), No. 1-2, p. 1.

[6] M.S. El-Eskandarany, *Mechanical Alloying for Fabrication of Advanced Engineering Materials*, Noyes Publications/William Andrew Publishing, Norwich, N.Y., 2001, p. 154.

[7] M.S. Khoskhoo, S. Scudinio, J. Thomas, K.B. Sureddi, and J. Eckert, Grain and crystalline size evaluation of cryomilled pure copper, *J. Alloys Compd.*, 509(2011), p. S343.

[8] H. Abdoli, H. Farnoush, E. Salahi, and K. Pourazrang, Study of the densification of a nanostructured composite powder Part 1: effect of compaction pressure and reinforcement addition, *Mater. Sci. Eng. A*, 486(2008), No. 1-2, p. 580.

[9] J. Ghosh, S. Mazumdar, M. Das, S. Ghatak, and A.K. Basu, Microstructural characterization of amorphous and nanocrystalline boron nitride prepared by high-energy ball milling, *Mater. Res. Bull.*, 43(2008), No. 4, p. 1023.

[10] J. Torrens-Serra, I. Peral, J. Rodriguez-Viejo, and M.T. Clavaguera-Mora, Microstructure evolution and grain size distribution in nanocrystalline FeNbBCu from synchrotron XRD and TEM analysis, *J. Non-Cryst. Solids*, 358(2012), No. 1, p. 107.

[11] F. Hadef, A. Otomani, A. Djekoun, and J.M. Grenèche, Structural and microstructural study of nanostructured $Fe_{50}Al_{40}Ni_{10}$ powders produced by mechanical alloying, *Mater. Charact.*, 62(2011), No. 8, p. 751.

[12] H. Dutta, A. Sen, J. Bhattacharjee, and S.K. Pradhan, Preparation of ternary $Ti_{0.9}Ni_{0.1}C$ cermets by mechanical alloying: microstructure characterization by Rietveld method and electron microscopy, *J. Alloys Compd.*, 493(2010), No. 1-2, p. 666.

[13] A. Inoue, Bulk amorphous alloys, [in] *Amorphous and Nanocrystalline Materials*, Springer, Berlin, 2001, p. 1.

[14] S.Z. Kou, L. Feng, Y.T. Ding, G.J. Xu, Z.F. Ding, and P.Q. La, Synthesis and magnetic properties of Cu-based amorphous alloys made by mechanical alloying, *Intermetallics*, 12(2004), No. 10-11, p. 1115.

[15] G.M. Wang, S.S. Fang, X.S. Xiao, Q. Hua, J.Z. Gu, and Y.D. Dong, Microstructure and properties of $Zr_{65}Al_{10}Ni_{10}Cu_{15}$ amorphous plates rolled in the supercooled liquid region, *Mater. Sci. Eng. A*, 373(2004), No. 1-2, p. 217.

[16] M. Gögebakan, The effect of Si addition on crystallization behaviour of amorphous Al–Y–Ni alloy, *J. Mater. Eng. Perform.*, 13(2004), No. 4, p. 504.

[17] R.S. Lei, M.P. Wang, H.P. Wang, and S.Q. Xu, New insights on the formation of supersaturated Cu–Nb solid solution prepared by mechanical alloying, *Mater. Charact.*, 118(2016), p. 324.

[18] M.A. Morris and D.G. Morris, Microstructure refinement and associated strength of copper alloys obtained by mechanical alloying, *Mater. Sci. Eng. A*, 111(1989), p. 115.

[19] A. Benghalem and D.G. Morris, Microstructure and mechanical properties of concentrated alloys prepared by mechanical alloying, *Mater. Sci. Eng. A*, 161(1993), No. 2, p. 255.

[20] E. Botcharova, M. Heilmaier, J. Freudenberger, G. Drew, D. Kudashow, U. Martin, and L. Schultz, Supersaturated solid solution of niobium in copper by mechanical alloying, *J. Alloys Compd.*, 351(2003), No. 1-2, p. 119.

[21] E. Botcharova, J. Freudenberger, and L. Schultz, Cu–Nb alloys prepared by mechanical alloying and subsequent heat treatment, *J. Alloys Compd.*, 365(2004), No. 1-2, p. 157.

[22] S. Mula, H. Bahmanpour, S. Mal, P.C. Kang, M. Atwater, W. Jian, R.O. Scattergood, and C.C. Koch, Thermodynamic feasibility of solid solubility extension of Nb in Cu and their thermal stability, *Mater. Sci. Eng. A*, 539(2012), p. 330.

[23] R.S. Lei, M.P. Wang, Z. Li, H.G. Wei, W.C. Yang, Y.L. Jia, and S. Gong, Structure evolution and solid solubility extension of copper–niobium powders during mechanical alloying,

Mater. Sci. Eng. A, 528(2011), No. 13-14, p. 4475.

[24] M. Azabou, H.I. Gharsallah, L. Escoda, J.J. Suñol, A.W. Kolsi, and M. Khitouni, Mechanochemical reactions in nanocrystalline Cu–Fe system induced by mechanical alloying in air atmosphere, *Powder Technol.*, 224(2012), p. 338.

[25] M. Khitouni, R. Daly, M. Mhadhbi, and A. Kolsi, Structural evolution in nanocristalline Cu obtained by high energy mechanical milling: phases formation of copper oxides, *J. Alloys Compd*., 475(2009), No. 1-2, p. 581.

[26] S.M. Yoon, C. Nagarjuna, D.W. Shin, C.H. Lee, B. Madavali, S.J. Hong, and K.H. Lee, Influence of milling atmosphere on thermoelectric properties of p-type Bi–Sb–Te based alloys by mechanical alloying, *J. Korean Powder Metall. Inst.*, 24(2017), No. 5, p. 357.

[27] Z.Q. Zhao, Z. Xiao, Z. Li, M.N. Zhu, and Z.Q. Yang, Characterization of dispersion strengthened copper alloy prepared by internal oxidation combined with mechanical alloying, *J. Mater. Eng. Perform.*, 26(2017), No. 11, p. 5641.

[28] M. do Carmo Amorim da Silva and S.J.G. de Lima, Evolution of mechanical alloying to obtain Cu–Al–Nb shape memory alloy, *Mater. Res.*, 8(2005), No. 2, p. 169.

[29] L. Lutterotti, S. Matthies, and H. R. Wenk, MAUD: a friendly Java program for material analysis using diffraction, *IUCr: Newsletter of the CPD*, 21(1999), p.14.

[30] J. Eckert, J.C. Holzer, and W.L. Johnson, Thermal stability and grain growth behavior of mechanically alloyed nanocrystalline Fe–Cu alloys, *J. Appl. Phys.*, 73(1993), No. 1, p. 131.

[31] F.A. Mohamed, A dislocation model for the minimum grain size obtainable by milling, *Acta Mater.*, 51(2003), No. 14, p. 4107.

[32] T. Bachaga, R. Daly, L. Escode, J.J. Suñol, and M. Khitouni, Amorphization of $Al_{50}(Fe_2B)_{30}Nb_{20}$ mixture by mechanical alloying, *Metall. Mater. Trans. A*, 44(2013), No. 10, p. 4718.

[33] M. Krifa, M. Mhadhbi, L. Escoda, J. Saurina, J.J. Suñol, N. LIorca-Isern, C. Artieda-Guzmán, and M. Khitouni, Phase transformation during mechanical alloying of Fe–30% Al–20% Cu, *Powder Technol.,* 246(2013), p. 117.

[34] H.I. Gharsallah, T. Makhlouf, L. Escoda, J.J. Suñol, and M. Khitouni, Magnetic and microstructural proprieties of nanocrystalline Fe–25at% Al and Fe–25at% Al + 0.2at% B alloys prepared by mechanical alloying process, *Eur. Phys. J. Plus*, 131(2016), No. 7, p. 119.

[35] S. Bergheul, H. Tafat, and M. Azzaz, Formation and magnetic properties of nanocrystalline $Fe_{60}Co_{40}$ alloys produced by mechanical alloying, *J. Mater. Eng. Perform.*, 15(2006), No. 3, p. 349.

[36] D.Y. Ying, and D.L. Zhang, Processing of Cu–Al_2O_3 metal matrix nanocomposite materials by using high energy ball milling, *Mater. Sci. Eng. A*, 286(2000), No. 1, p. 152.

[37] M. Gherib, A. Otmani, A. Djekoun, A. Bouasla, M. Poulain, and M. Legouira, Study of nanocrystalline NiAl alloys prepared by mechanical alloying, *Defect Diffus. Forum*, 329(2012), p. 19.

[38] Y.C. Zhang, J.Y. Tang, G.L. Wang, M. Zhang, and X.Y. Hu, Facile synthesis of submicron Cu_2O and CuO crystallites from a solid metallorganic molecular precursor, *J. Cryst. Growth*, 294(2006), No. 2, p. 278.

[39] M.D. Abad, S. Parker, D. Kiene, M.M. Primorac, and P. Hosemann, Microstructure and mechanical properties of Cu_xNb_{1-x} alloys prepared by ball milling and high pressure torsion compacting, *J. Alloys Compd.*, 630(2015), p. 117.

[40] W. Pfeiler, *Alloy Physics: A Comprehensive Reference*, John Wileys and Sons, New York, 2008.

[41] R.S. Lei, S.Q. Xu, M.P. Wang, and H.P. Wang, Microstructure and properties of nanocrystalline copper–niobium alloy with high strength and high conductivity, *Mater. Sci. Eng. A*, 586(2013), p. 367.

[42] M. Slimi, M. Azabou, L. Escoda, J.J. Suñol, and M. Khitouni, Stacking faults and structural characterization of mechanically alloyed $Ni_{50}Cu(Fe_2B)_{10}P_{30}$ powders, *Eur. Phys. J. Plus*, 130(2015), No. 4, p. 72.

[43] S. Sivasankaran, K. Sivaprasad, R. Narayanasamy, and P.V. Satyanarayana, X-ray peak broadening analysis of AA 6061_{100-x}–x wt.% Al_2O_3 nanocomposite prepared by mechanical alloying, *Mater. Charact.*, 62(2011), No. 7, p. 661.

[44] Y.H. Zhao, H.W. Sheng, and K. Lu, Microstructure evolution and thermal properties in nanocrystalline Fe during mechanical attrition, *Acta Mater.*, 49(2001), No. 2, p. 365.

[45] C. Slama and M. Abdellaoui, Microstructure characterization of nanocrystalline ($Ti_{0.9}W_{0.1}$) C prepared by mechanical alloying, *Int. J. Refract. Met. Hard Mater.*, 54(2016), p. 270.

[46] M. Slimi, M. Azabou, L. Escoda, J.J. Suñol, and M. Khitouni, Structural and microstructural properties of nanocrystalline Cu–Fe–Ni powders produced by mechanical alloying, *Powder Technol.*, 266(2014), p. 262.

[47] I. Hideaki, M. Toshiyuki, and N. Keiji, Measurement of enthalpies of formation of niobium oxides at 920 K in a Tian-Calvet-type calorimeter, *J. Chem. Thermodyn.*, 16(1984), No. 5, p. 411.

[48] K.T. Jacob, C. Shekhar, M. Vinay, and Y. Waseda, Thermodynamic properties of niobium oxides, *J. Chem. Eng. Data*, 55(2010), No 11, p. 4854.

[49] R. Novakovic, Thermodynamics, surface properties and microscopic functions of liquid Al–Nb and Nb–Ti alloys, *J. Non-Cryst. Solids,* 356(2010), No. 31-32, p. 1593.